

Magnetic Sponge Prepared with an Alkanedithiol-Bridged Network of Nanomagnets

Yoshikazu Ito,[†] Akira Miyazaki,[‡] Kazuyuki Takai,[†] Vajiravelu Sivamurugan,[§] Takashi Maeno,^{||} Takeshi Kadono,[⊥] Masaaki Kitano,[#] Yoshihiro Ogawa,^{||} Naotake Nakamura,[∇] Michikazu Hara,^{⊥,#} Suresh Valiyaveetil,[§] and Toshiaki Enoki^{*,†}

[†]Department of Chemistry, Graduate School of Science and Engineering, Tokyo Institute of Technology, 2-12-1 Ookayama, Meguro-ku, Tokyo 152-8551, Japan

[‡]Department of Environmental Applied Chemistry, Faculty of Engineering, University of Toyama, 3190 Gofuku, Toyama-shi, Toyama 930-8555, Japan

[§]Department of Chemistry, National University of Singapore, 3 Science Drive 3, Singapore 117543

^{||}Department of Chemistry, Graduate School of Science and Technology, Kumamoto University, 2-39-1 Kurokami, Kumamoto 860-8555, Japan

[⊥]Kanagawa Academy of Science and Technology, 3-2-1 Sakado, Takatsu-ku, Kawasaki 213-0012, Japan

[#]Materials and Structures Laboratory, Tokyo Institute of Technology, 4259 Nagatsuta, Midori-ku, Yokohama 226-8503, Japan

[∇]Institute for General Education, Ritsumeikan University, 1-1-1 Nojihigashi, Kusatsu, Shiga 525-8577, Japan

S Supporting Information

ABSTRACT: The magnetic dipole–dipole interaction between nanomagnets having huge magnetic moments can have a strength comparable to that of the van der Waals interaction between them, and it can be manipulated by applying an external magnetic field of conventional strength. Therefore, the cooperation between the dipole–dipole interaction and the applied magnetic field allows the magnetic moments of nanomagnets to be aligned and organized in an ordered manner. In this work, a network of magnetic nanoparticles connected with flexible long-alkyl-chain linkers was designed to develop a “magnetic sponge” capable of absorbing and desorbing guest molecules with changes in the applied magnetic field. The magnetization of the sponge with long-alkyl-chain bridges (30 C atoms) exhibited a 500% increase after cooling in the presence of an applied field of 7 T relative to that in the absence of a magnetic field. Cooling in a magnetic field leads to anisotropic stretching in the sponge due to reorganization of the nanomagnets along the applied field, in contrast to the isotropic organization under zero-field conditions. Such magnetic-responsive organization and reorganization of the magnetic particle network significantly influences the gas absorption capacity of the nanopores inside the material. The absorption and desorption of guests in an applied magnetic field at low temperature can be regarded as a fascinating “breathing feature” of our magnetic sponge.

“Magnetic sponges”^{1–5} fabricated from flexible structures of magnetic metal complexes help us understand the fundamental aspects of host–guest interactions in a gas absorption mechanism and have industrial applications as molecular sieves, sensors, and ion exchangers and in gas storage, catalytic reaction sites, and drug delivery systems. Their flexible structure

is easily expanded/contracted upon absorption/desorption of guest molecules such as water or gases. Accordingly, magnetic sponges with flexible frameworks and magnetic metal centers offer fascinating magnetic properties that can be modified depending on the reversible structural changes induced by reversible guest absorption/desorption. However, there has been no report of a magnetic sponge whose structure can be changed reversibly by the application of an external magnetic field. In this work, a combination of gas absorption and an external magnetic field allowed us to control the structure–property–function triad of the magnetic sponge and showed a lattice breathing phenomenon related to absorption and desorption of gases.

This paper describes a magnetic sponge that exhibits expansion/contraction of its framework with changes in the applied magnetic field, as illustrated in Figure 1. The magnetic dipole–dipole interaction U given in eq 1 is sensitive to the directions of the magnetic dipoles at sites i and j (μ_i and μ_j , respectively):

$$U = \frac{\mu_i \mu_j (1 - 3 \cos^2 \theta)}{r_{ij}^3} \quad (1)$$

where μ_i and μ_j are the magnitudes of μ_i and μ_j , respectively, r_{ij} is the magnitude of the vector \mathbf{r}_{ij} connecting i and j , and θ is the tilt angle of \mathbf{r}_{ij} . When the two dipoles with their directions aligned antiparallel (antiferromagnetic)/parallel (ferromagnetic) are arranged side-by-side ($\theta = 90^\circ$), an attractive/repulsive potential with a strength of $\mu_i \mu_j / r_{ij}^3$ operates between them. In contrast, in the case of a head-to-tail arrangement ($\theta = 0^\circ$), an attractive/repulsive potential with a strength of $2\mu_i \mu_j / r_{ij}^3$ operates between the two dipoles aligned parallel/antiparallel. Accordingly, when the applied magnetic field forces the dipoles to align along the field direction, the intermagnet distance in the side-by-side direction (the X direction in Figure 1) increases, which leads

Received: May 19, 2011

Published: July 06, 2011

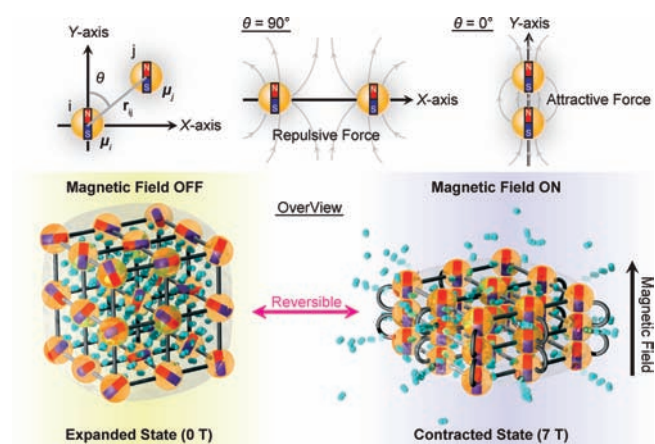


Figure 1. Expanded and contracted states of the magnetic sponge. Upper panel: Geometrical relation of two dipoles, μ_i at site i (located at the origin) and μ_j at site j . The vector r_{ij} connects i and j and makes an angle θ with respect to the X axis. Lower panel: Orange spheres represent nanomagnet particles of a 3 nm Co–Pd alloy, and blue spheres represent nitrogen molecules. The black arrow represents the direction of the applied magnetic field. An expanded state with the nanopores filled with nitrogen is formed in the absence of the magnetic field (0 T), in which the magnetic dipoles of the constituent nanomagnets are randomly oriented. A contracted state from which the nitrogen has been expelled is formed upon application of the magnetic field (7 T), in which all of the dipoles are oriented along the field direction. The two states are reversibly transformed by switching the magnetic field on/off. The nitrogen molecules serve to maintain the structure in the contracted/expanded state.

to extension of the alkyl chains, whereas the distance along the head-to-tail direction (the Y direction in Figure 1) decreases, which causes compression of the alkyl chains. Hence, the application of the field compresses the entire network anisotropically and expels the absorbed guest molecules from its nanopores. In contrast, in the absence of a magnetic field, the network remains expanded with its nanopores filled with guest molecules. Such interesting magnetic-field-induced “breathing” of a magnetic sponge has not been observed in existing systems.

Magnetic Co–Pd alloy nanoparticles⁶ were used as the network connector points of the flexible alkyl chains of the magnetic sponge because of their giant magnetic moments and chemical stability. According to our previous study,⁶ the magnetic moment of a Co–Pd alloy nanoparticle is strongly enhanced by exchange enhancement.⁷ Furthermore, the Pd atoms protect the Co atoms from air oxidation when the atomic concentration of Co is less than 32 atom %.^{6a} Icosane-1,20-dithiol (C_{20} dithiol)^{8,9} and triacontane-1,30-dithiol (C_{30} dithiol), which have chain lengths of 2.5–3.0 nm and 3.8–4.5 nm, respectively, were employed as bridging molecules.

The sponge was characterized using elemental analysis (EA), transmission electron microscopy (TEM), and the nitrogen absorption/desorption method. In the TEM image shown in Figure 2a, well-dispersed Co–Pd alloy nanoparticles (16 atom % Co by EA) can be observed as homogeneous spheres before the cross-linking. The diameters estimated from the TEM images were 3.0 ± 0.3 and 3.0 ± 0.4 nm for the 16 atom % Co (C_{20} dithiol) and 18 atom % Co (C_{30} dithiol) nanoparticles, respectively. The lattice image (inset, spacing = 0.2 nm) was assigned to the (111) planes of the Pd face-centered cubic (fcc) lattice, which is consistent with the equilibrium phase diagram of bulk Co–Pd

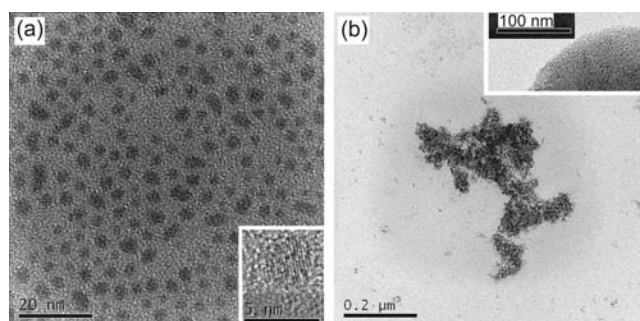


Figure 2. TEM images of the magnetic sponge (a) before and (b) after cross-linking. (a) The average diameter of the well-dispersed nanoparticles was 3.0 ± 0.3 nm before cross-linking (scale bar: 20 nm). The inset (scale bar: 5 nm) shows a magnified view of the lattice spacing (0.2 nm). (b) The well-dispersed nanoparticles formed agglomerates after cross-linking (scale bar: $0.2 \mu\text{m}$). The inset (scale bar: 100 nm) presents a magnified view showing well-packed nanoparticles.

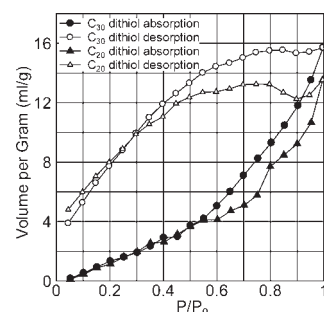


Figure 3. Nitrogen absorption and desorption isotherms at 77 K for the magnetic sponges containing C_{20} dithiols (triangles) and C_{30} dithiols (circles). The vertical axis represents the volume of nitrogen (gas) per gram and the horizontal axis the value of P/P_0 (where $P_0 = 0.10$ MPa is the vapor pressure of nitrogen at 77.4 K). Open and solid symbols represent nitrogen absorption and desorption, respectively. The maximum volumes of absorbed nitrogen are 13.5 mL/g for the C_{20} dithiol magnetic sponge and 15.7 mL/g for the C_{30} dithiol magnetic sponge.

alloy.¹⁰ From the lattice parameter of bulk fcc Pd ($a_0 = 0.3891$ nm),¹¹ the average number of metal atoms per particle was estimated to be 950–1050. The well-dispersed nanoparticles formed large aggregates after cross-linking with alkanedithiol molecules (Figure 2b). Well-packed nanoparticles were observed at the edge of an aggregate (inset). Thus, it is conceivable that the aggregates comprise a large number of nanoparticles mutually linked by alkanedithiol molecules.

From the nitrogen absorption/desorption isotherms shown in Figure 3, the specific surface areas of the C_{20} dithiol- and C_{30} dithiol-bridged nanoparticles were estimated to be $10 \text{ m}^2/\text{g}$ using the BET formula,¹² and their corresponding maximum absorption volumes at $P/P_0 = 1$ were 13 and 16 mL/g, respectively. This suggests that the framework with C_{30} dithiols can absorb a higher number of gas molecules in the nanopores than that of the sponge incorporating C_{20} dithiols.

The magnetizations of the nanoparticles were measured using a SQUID magnetometer by a reported method.^{6,13} The sponges containing 16 atom % Co nanoparticles/ C_{20} dithiol and 18 atom % Co nanoparticles/ C_{30} dithiol exhibited saturation magnetizations of $340 \mu_B$ and $450 \mu_B$ at 2 K and superparamagnetic blocking temperatures¹⁴ of 4 and 3 K, respectively. To confirm

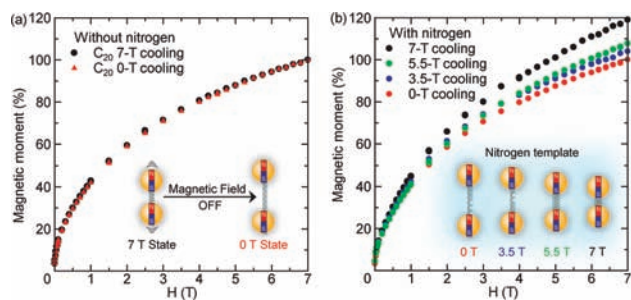


Figure 4. (a) Magnetization curves of the 16 atom % Co/C₂₀ dithiol magnetic sponge under vacuum conditions at 2 K. Black circles and red triangles represent magnetization curves under field-cooling (7 T) and zero-field-cooling (0 T) conditions, respectively, with the nanopores being empty ($P \approx 10^{-5}$ Pa). The magnetization at 7 T was 14.0 emu/g. (b) Magnetization curves of the 16 atom % Co/C₂₀ dithiol magnetic sponge in the field-cooled samples at different magnetic field strengths with the nanopores filled with nitrogen. Red, blue, orange, and black circles represent magnetization curves after cooling at 0, 3.5, 5.5, and 7 T, respectively. The inset shows that nitrogen molecules (aqua) serve to keep their expanded or contracted states at low temperature. The values are normalized to the magnetization of the zero-field-cooled sample at 7 T (14.8 emu/g).

the sponge performance, the effects of nitrogen absorption and field cooling were tested (Figure 4). Without nitrogen absorbed in the pores (the sample was evacuated at $P \approx 10^{-5}$ Pa at 300 K for 72 h), the magnetization curves of the 16 atom % Co/C₂₀ dithiol framework exhibited no significant difference between zero-field-cooling

(0 T) and field-cooling (7 T) conditions, as shown in Figure 4a. However, with absorbed nitrogen inside the sponge, the curves clearly depended on the field applied during cooling, as shown in Figure 4b. Indeed, the magnetization of the 7 T field-cooled sample at low temperature was 20% larger than that of the zero-field-cooled sample. This enhancement is caused by the cooperation of the applied magnetic field and the magnetic dipole–dipole interaction, which reorganizes the nanoparticles and sponge lattice anisotropically. In the presence of an external magnetic field, the magnetic moments of all of the nanoparticles in an aggregate are forced to be aligned with the field direction. Accordingly, the internanoparticle distance along the field direction decreases because of a strong attractive interaction, while the distance perpendicular to the field direction increases because of a repulsive interaction. Consequently, the magnetic moments are strongly coupled along the field direction at the expense of thermal fluctuations and behave like a single giant magnetic moment, resulting in an increase in the magnetization. The changes in the magnetization at low temperature are proportional to the strength of applied magnetic field (Figure 4b), and the observed increase in the magnetization indicates field-induced anisotropic compression of the sponge framework.

To demonstrate that the flexible dithiol spacer is a key to breathing, the magnetizations for a network synthesized using a rigid oligo(phenylene ethynylene) diethanethioate (OPE diethanethioate) spacer and for C₁₈ thiol-capped nanoparticles without any cross-linking (“pristine” nanoparticles) were investigated. The effects of cross-linking using flexible molecules (C₂₀ dithiol) or rigid molecules (OPE diethanethioate) were assessed by comparison with a non-cross-linked sample of pristine Co–Pd alloy nanoparticles (no network). The magnetization changes, which depend on the morphology changes, were investigated using a

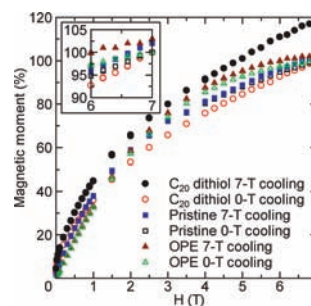


Figure 5. Cross-linking dependence of the magnetization curve of the Co–Pd nanoparticles (16 atom % Co) at 2 K. Squares, circles, and triangles represent pristine nanoparticles (no cross-linking), nanoparticles cross-linked with C₂₀ dithiols, and nanoparticles cross-linked with OPE diethanethioate, respectively. Solid and open symbols denote the results after cooling at 7 and 0 T, respectively.

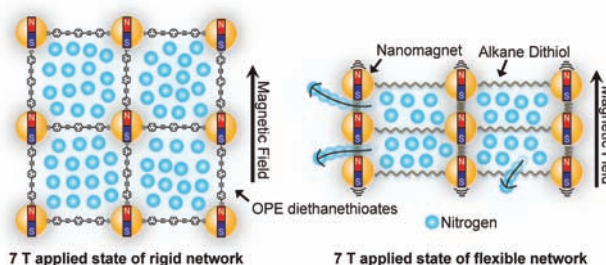


Figure 6. Schematic illustrations of the rigid and flexible networks under a 7 T applied magnetic field.

SQUID with the cooling procedure described in the Supporting Information (SI). Figure 5 presents the cross-linking dependence of the magnetization curve of Co–Pd alloy nanoparticles (16 atom % Co). Only the flexible network showed an effective difference between the zero-field-cooling and field-cooling data, whereas the rigid network and the samples with no network showed little difference. Because of the rigid network, the OPE diethanethioates resist the anisotropic stretches generated by the magnetic dipole–dipole interaction in the 7 T magnetic field, which is the highest in the present experiment. In the case of the pristine nanoparticles with no network, the assembly of the nanoparticles cannot form an anchored structure and an anchored nanopore system, and furthermore, it is conceivable that the non-anchored nanoparticles rearrange themselves into an energetically stable state through the strong magnetic dipole–dipole interaction. Therefore, only the flexible cross-linking molecules form the magnetic sponge. These differences under the 7 T applied magnetic field are illustrated in the schematic image in Figure 6. Neither the rigid framework nor the pristine sample exhibited the breathing phenomena observed with sponges incorporating the flexible alkanedithiols.

When the chain length of the organic spacer molecules was increased from C₂₀ to C₃₀, the magnetization was significantly enhanced under field cooling. The magnetization curves (for 18 atom % Co/C₃₀ dithiol) were independent of the applied field in the absence of nitrogen molecules (Figure S1 in the SI). Interestingly, in the presence of nitrogen inside the sponge, the magnetization at 7 T after 7 T field cooling was enhanced by 500% in comparison with the magnetization measured at 2 K after zero-field cooling (Figure 7a). This enhancement was significantly larger than that exhibited by the framework having shorter

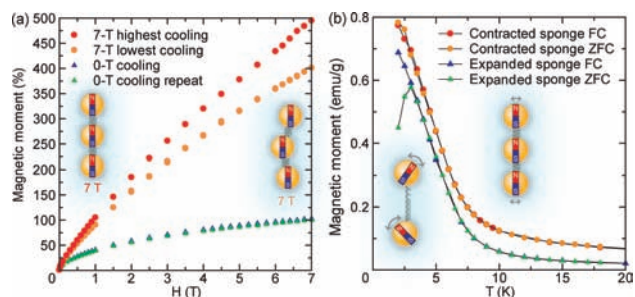


Figure 7. (a) Magnetization curve of the 18 atom % Co/C₃₀ dithiol magnetic sponge at 2 K. Red and orange circles represent magnetization curves after field-cooling at 7 T; blue and green triangles represent magnetization curves after zero-field cooling. The vertical axis is normalized to the magnetic moment at 7 T after zero-field cooling (17.5 emu/g). The magnetization values under 7 T field cooling were scattered for repeated runs for the same sample. The magnetization curves with highest and lowest magnetizations are plotted. (b) Temperature dependence of the magnetization of the 18 atom % Co/C₃₀ dithiol magnetic sponge measured at 10 mT. Circles represent the magnetizations of the sponge contracted in 7 T field cooling; triangles represent magnetizations of the sponge expanded in 0 T cooling. Orange and green symbols denote zero-field cooling (ZFC) and red and blue symbols field cooling (FC) at 7 T after annealing at 50 K without an external field (see the SI).

alkanedithiol linkers (e.g., C₂₀ dithiols) (Figure 4b). Also, this enhancement was scattered, with a deviation of 30% over several repeated runs of the 7 T field-cooling process for the same sample (Figure 7a). These results can be explained by the anisotropic contraction of the network (Figure 1). As the C₃₀ dithiol spacer is more flexible than the C₂₀ dithiol one, the structural change becomes more significant. Accordingly, the structure of the final contracted state can depend on small uncontrollable perturbations during the field-cooling process; hence, the magnetization at a low temperature cannot have a definite value and is somewhat scattered, possibly depending on the number of defects in the contracted structure.

Furthermore, the temperature dependence of the magnetization (Figure 7b) gives important evidence of expansion/contraction of the framework. The sample was first cooled to 2 K at 0 or 7 T and then warmed to 50 K (which is below the nitrogen boiling point at ~77 K) at 0 T, after which measurements were performed at 10 mT (see the SI) after cooling at 0 T. The zero-field-cooled sample exhibited a blocking temperature of 3 K for the expanded framework, whereas this blocking phenomenon disappeared in the same sample cooled in a field of 7 T. This in the expanded framework is similar to the blocking behavior of a superparamagnet. In contrast, the same sample with the contracted framework did not show any blocking behavior irrespective of the cooling conditions, which is caused by the dipolar field generated by the contracted structure.

In conclusion, we have prepared and characterized magnetic nanoparticle/alkyl chain frameworks (i.e., magnetic Co–Pd alloy nanoparticles cross-linked with C₂₀ or C₃₀ dithiols) for the design of a flexible network of magnetic nanoparticles that can be expanded and contracted using an external magnetic field. It has been demonstrated that expansion and contraction of this network can be induced by the magnetic dipole–dipole interaction in the presence of an applied magnetic field with the assistance of nitrogen absorption/desorption. The magnetic sponge framework achieves a 500% enhancement in the magnetization in the contracted state relative to the expanded state.

This phenomenon is an interesting “magnetic sponge” effect that has not been reported previously.

■ ASSOCIATED CONTENT

S Supporting Information. Details of materials and methods, synthetic procedures for magnetic sponges, procedure for cooling samples, magnetization curve for the C₃₀ dithiol magnetic sponge under vacuum, and NMR data for new molecules. This material is available free of charge via the Internet at <http://pubs.acs.org>.

■ AUTHOR INFORMATION

Corresponding Author

enoki.t.aa@m.titech.ac.jp

■ ACKNOWLEDGMENT

This work was supported by a Grant-in-Aid for Scientific Research (15073211) and the “Nanotechnology Support Project” of the Ministry of Education, Culture, Sports, Science and Technology (MEXT), Japan, and by the Agency for Science, Technology and Research (ASTAR), Singapore. Y.I. was supported by a JSPS Fellowship. The authors thank Dr. K. Yokota for valuable discussions.

■ REFERENCES

- (1) Ohkoshi, S.; Arai, K.; Sato, Y.; Hashimoto, K. *Nat. Mater.* **2004**, *3*, 857.
- (2) Maspoche, D.; Ruiz-Molina, D.; Wurst, K.; Domingo, N.; Cavallini, M.; Biscarini, F.; Tejada, J.; Rovira, C.; Veciana, J. *Nat. Mater.* **2003**, *2*, 190.
- (3) Ghosh, S. K.; Kaneko, W.; Kiriyama, D.; Ohba, M.; Kitagawa, S. *Angew. Chem., Int. Ed.* **2008**, *47*, 8843.
- (4) Kahn, O.; Larionova, J.; Yakhmi, J. V. *Chem.—Eur. J.* **1999**, *5*, 3443.
- (5) Férey, G. *Chem. Mater.* **2001**, *13*, 3084.
- (6) (a) Ito, Y.; Miyazaki, A.; Fukui, K.; Valiyaveetil, S.; Yokoyama, T.; Enoki, T. *J. Phys. Soc. Jpn.* **2008**, *77*, No. 103701. (b) Miyazaki, A.; Ito, Y.; Enoki, T. *Eur. J. Inorg. Chem.* **2010**, 4279. (c) Ito, Y.; Takai, K.; Enoki, T. *J. Phys. Chem. C* **2011**, *15*, 8971.
- (7) Moriya, T. *Prog. Theor. Phys.* **1965**, *34*, 329.
- (8) Nakamura, N.; Uno, K.; Ogawa, Y. *Acta Crystallogr.* **2001**, *E57*, o505.
- (9) Kuwabara, K.; Horii, F.; Ogawa, Y. *J. Mol. Struct.* **2002**, *602–603*, 79.
- (10) Ishida, K.; Nishizawa, T. *J. Phase Equilib.* **1991**, *12*, 83.
- (11) Mueller, M. F.; Freeman, A. J.; Dimmock, J. O.; Furdyna, A. M. *Phys. Rev. B.* **1970**, *1*, 4617.
- (12) Brunauer, S.; Emmett, P. H.; Teller, E. *J. Am. Chem. Soc.* **1938**, *60*, 309.
- (13) Ito, Y.; Miyazaki, A.; Valiyaveetil, S.; Enoki, T. *J. Phys. Chem. C* **2010**, *114*, 11699.
- (14) Bedanta, S.; Kleemann, W. *J. Phys. D: Appl. Phys.* **2009**, *42*, No. 013001.